Int. J. Electrochem. Sci., 8 **(2013)** 2262 - 2271

International Journal of
ELECTROCHEMICAL
SCIENCE
www.electrochemsci.org

Microstructures and Electrochemical Hydrogen Storage Characteristics of $La_{0.65-x}Ce_{0.25-x}Pr_{0.03}Nd_{0.07}Y_{2x}Ni_{3.65}Co_{0.75}Mn_{0.3}Al_{0.3}$ (x = 0-0.04) Alloys

Xianyun Peng[1], *Baozhong Liu*[1,*], *Yu Zhou*[2], *Yanping Fan*[1], *Yonggang Yang*[2], *Qian Li*[2]

[1] School of Materials Science & Engineering, Henan Polytechnic University, Jiaozuo 454000, China
[2] Inner Mongolia Rare Earth Ovonic Metal Hydride Co. Ltd., Baotou 014030, China
[*]E-mail: bzliu@hpu.edu.cn

Received: 13 December 2012 / *Accepted:* 5 January 2013 / *Published:* 1 February 2013

Microstructures and electrochemical hydrogen storage characteristics of $La_{0.65-x}Ce_{0.25-x}Pr_{0.03}Nd_{0.07}Y_{2x}Ni_{3.65}Co_{0.75}Mn_{0.3}Al_{0.3}$ alloys have been investigated. All alloys exhibit the diffraction peaks corresponding to the single $LaNi_5$ phase with $CaCu_5$ structure, and lattice parameters a, c and cell volume V decrease with increasing x value. Activation performance and maximum discharge capacity degrade with increasing x from 0 to 0.04. High-rate dischargeability at the discharge current density of 1200 mA/g decreases from 71.6% (x = 0) to 57.7% (x = 0.04), and shows a linear relationship with hydrogen diffusion coefficient. S_{500} increases from 67.9% (x = 0) to 80.1% (x = 0.04), which should be ascribed to the improvement of corrosion resistance due to the addition of yttrium.

Keywords: Hydrogen storage alloy; Phase structure; Cycling stability; Electrochemical kinetics; Ni-MH battery

1. INTRODUCTION

AB_5-type (Original $LaNi_5$) hydrogen storage alloys are widely used as the negative electrode materials in commercial nickel/metal hydride (Ni/MH) batteries due to their good activation ability, high capacity, high resistance to overcharging and overdischarging, high rate charge/discharge performance, long cycle life and environmental friendliness, etc [1-3]. However, in recent years, Ni/MH batteries have been confronted with the rapid development of other devices, rapidly developing towards the lower cost and the high performance [4]. Cycle life is a critical criterion of evaluating the electrochemical hydrogen storage property as negative electrode because long cycle life can increase the ratio of performance to price and then improve the market competitiveness of Ni/MH battery [5].

Thus, it is very imperative to further improve the cycling stability of AB_5-type hydrogen storage alloys.

It is well-known that element substitution is an effective way to improve the electrochemical properties of AB_5-type hydrogen storage alloy. The partial substation of La in A side by Ce, Pr, Nd, and partial substitution of Ni in B side by Co, Mn, Al have been extensively investigated[6]. Ye et al. [7] reported that the electrochemical properties of AB_5-type alloy successfully modified by adjusting the rare earth composition in A side. Mukerjee et al. [8] reported that the substation of La by Ce can effectively improve the cycling stability of AB_5-type alloy due to the formation of a passivating Ce oxide. Maurel et al. [9] reported that the addition of Y_2O_3 in electrolyte can decrease corrosion rate of alloy electrode due to a decrease of the driving force for diffusion of $Mm^{3+}$and OH^-. Moreover, Ticianelli et al.[10] reported that the alloying with Y decreased the corrosion rate due to forming a physical barrier of Y hydrous oxide, which acts as a blocking passivating layer. Based on above results, the improvement of cycling stability by adjusting rare earth composition is expected. In this paper, $La_{0.65}Ce_{0.25}Pr_{0.03}Nd_{0.07}Ni_{3.65}Co_{0.75}Mn_{0.3}Al_{0.3}$ was selected as a base alloy because it was a typical commercial AB_5-type alloy with high discharge capacity and excellent high-rate dischargeability. $La_{0.65-x}Ce_{0.25-x}Pr_{0.03}Nd_{0.07}Y_{2x}Ni_{3.65}Co_{0.75}Mn_{0.3}Al_{0.3}$ alloys were prepared, and microstructure and electrochemical properties of alloy electrode were investigated in detail.

2. EXPERIMENTAL PROCEDURES

$La_{0.65-x}Ce_{0.25-x}Pr_{0.03}Nd_{0.07}Y_{2x}Ni_{3.65}Co_{0.75}Mn_{0.3}Al_{0.3}$ (x = 0-0.04) alloys were synthesized by induction melting of the metal elements (La, Ce, Pr, Nd, Y, Ni, Co, Mn, Al: 99.9% in purity) under argon atmosphere and then were annealed at 1123 K for 8 h.

The phases of the alloy powders were determined by X-ray diffraction (XRD) using a Rigaku D/max 2500PC powder diffractometer with Cu Kα radiation. The phase structures of alloys were analyzed using Jade-5 software.

The alloy powders of measuring electrodes were obtained by grinding the inner part of alloy ingots in the Ar atmosphere. All measuring electrodes for test were prepared by cold pressing the mixture of 0.15 g alloy powders of 200-400 meshes and 0.75 g nickel carbonyl powders into a pellet of 10 mm in diameter under 15 MPa. Electrochemical measurements were performed at 298 K in a standard tri-electrode system, consisting of a working electrode (metal hydride), a counter electrode ($Ni(OH)_2$/NiOOH), and a reference electrode (Hg/HgO) with 6 mol/L KOH solution as electrolyte. Each electrode was charged for 7 h at 60 mA/g and discharged to -0.6 V versus Hg/HgO at 60 mA/g at 298 K. After every charging/discharging, the rest time was 10 min. In evaluating the high-rate dischargeability, discharge capacity of the alloy electrodes at different discharge current density was measured. The high-rate dischargeability HRD (%) was defined as $C_d/C_{max} \times 100\%$, where C_d was the discharge capacity at the discharge current density I_d (I_d = 60, 300, 600, 900 and1200 mA/g, respectively), and C_{max} was the maximum discharge capacity at the discharge current density of 60 mA/g.

The electrochemical impedance spectrum (EIS) and potential-step measurement were obtained

by Advanced Potentiostat/Galvanostat (PARSTAT 2273). At 50% depth of discharge (DOD), the EIS was tested in the frequency range of 100 kHz to 10 mHz. For potential-step measurement, the electrodes in fully charged state were discharged with potential steps of 0.5 V for 3600 s.

3. RESULTS AND DISCUSSION

3.1 Crystal structure

Fig. 1 shows XRD patterns of $La_{0.65-x}Ce_{0.25-x}Pr_{0.03}Nd_{0.07}Y_{2x}Ni_{3.65}Co_{0.75}Mn_{0.3}Al_{0.3}$ alloys. It is clear that all alloys exhibit the diffraction peaks corresponding to the single $LaNi_5$ phase with $CaCu_5$ structure. The lattice parameters of the alloys were calculated and are listed in Table 1. It can be seen that lattice constant *a* and *c* decrease with increasing *x* value, and the cell volume *V* also decreases with increasing *x* value, which should be the smaller atomic radius of Y than that of La and Ce. Similar results is in agreement with the literature[11].

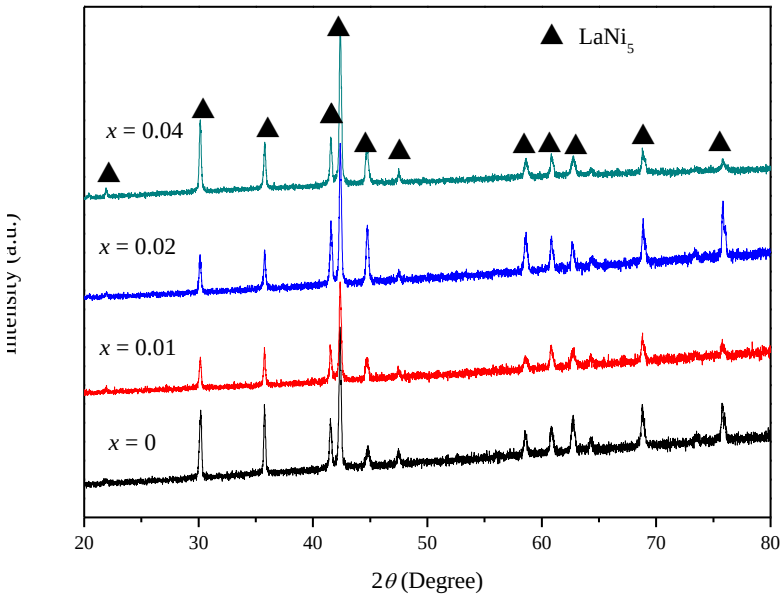

Figure 1. XRD patterns of $La_{0.65-x}Ce_{0.25-x}Pr_{0.03}Nd_{0.07}Y_{2x}Ni_{3.65}Co_{0.75}Mn_{0.3}Al_{0.3}$ alloys

Table 1. Lattice parameters of $La_{0.65-x}Ce_{0.25-x}Pr_{0.03}Nd_{0.07}Y_{2x}Ni_{3.65}Co_{0.75}Mn_{0.3}Al_{0.3}$ alloys

x	*a*/Å	*c*/Å	*V*/Å^3
0	5.019	4.050	88.35
0.01	5.017	4.050	88.28
0.02	5.013	4.044	88.01
0.04	5.012	4.043	87.95

3.2 Activation property and maximum discharge capacity

The number of cycles (N_a) needed to active the electrodes and maximum discharge capacity (C_{max}) of $La_{0.65-x}Ce_{0.25-x}Pr_{0.03}Nd_{0.07}Y_{2x}Ni_{3.65}Co_{0.75}Mn_{0.3}Al_{0.3}$ alloy electrodes are given in Table 2. N_a increases from 6 (x = 0) to 8 (x =0.04), indicating the activation property of alloy electrodes decreases with increasing x value. Generally, the activation performance of the alloy electrode is related with the surface electrochemical activity and internal energy [12]. Wu et al. [13] reported that the oxidation film on alloy surface increased the additive internal energy, and then degraded the activation performance. The increase of Y makes the surface oxidation become dense [10, 11] and therefore leads to the increase of internal energy, and then degrades activation performance. Moreover, dense oxidation on the alloy surface also is detrimental to the surface electrochemical activity of Y-containing alloy electrode, which is unfavorable to the activation property.

Table 2. Electrochemical properties of $La_{0.65-x}Ce_{0.25-x}Pr_{0.03}Nd_{0.07}Y_{2x}Ni_{3.65}Co_{0.75}Mn_{0.3}Al_{0.3}$ alloy electrodes

x	C_{max} (mAh/g)	N_a	HRD_{1200}[a] (%)	S_{500} (%)
0	322.95	6	71.6	67.9
0.01	319.75	7	65.4	74.5
0.02	310.35	7	62.0	76.7
0.04	304.70	8	57.7	80.1

[a] The high-rate dischargeability at the discharge current density of 1200 mA/g.

The C_{max} of alloy electrodes decrease from 322.95 mAh/g (x = 0) to 304.70 mAh/g (x = 0.04) with increasing x value. In general, the C_{max} is related with the crystalline structure and electrochemical kinetics of alloy electrode. Brateng er al. [14] pointed out that the discharge capacity has a linear relationship with the cell volume. The larger cell volume is, the discharge capacity is higher. The decrease in cell volume of alloys is detrimental to the discharge capacity. Moreover, Fig. 2 shows the dehydriding curves of $La_{0.65-x}Ce_{0.25-x}Pr_{0.03}Nd_{0.07}Y_{2x}Ni_{3.65}Co_{0.75}Mn_{0.3}Al_{0.3}$ alloy. Clearly the hydrogen capacity of alloys decreases with increasing x value, which is also unfavorable to the discharge capacity. In addition, It can be seen from fig. 2 that the plateau pressure of alloy increases with increasing x value, indicating the stability of alloy hydride increases with increasing Y content. The higher hydride stability makes the release of bonded hydrogen more difficult, which is detrimental to the hydrogen diffusion in the bulk alloy[15]. The increase of hydride stability with increasing x value will degrade the hydrogen diffusion in the bulky alloy, and is unbeneficial to the discharge capacity.

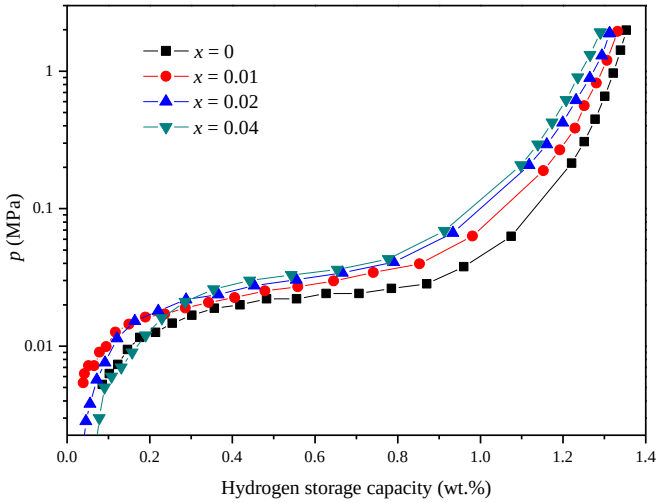

Figure 2. Dehydriding curves of $La_{0.65-x}Ce_{0.25-x}Pr_{0.03}Nd_{0.07}Y_{2x}Ni_{3.65}Co_{0.75}Mn_{0.3}Al_{0.3}$ alloy at 313 K

3.3 HRD and electrochemical kinetics

Fig. 3 shows the relationship between the HRD and the discharge current density of $La_{0.65-x}Ce_{0.25-x}Pr_{0.03}Nd_{0.07}Y_{2x}Ni_{3.65}Co_{0.75}Mn_{0.3}Al_{0.3}$ alloy electrodes. It can be seen that the HRD of alloy electrode decreases with increasing x from 0 to 0.04. The HRD at the discharge current density of 1200 mA/g (HRD_{1200}) is listed in Table 2. It can be seen that HRD_{1200} decreases from 71.6% (x = 0) to 57.7% (x = 0.04).

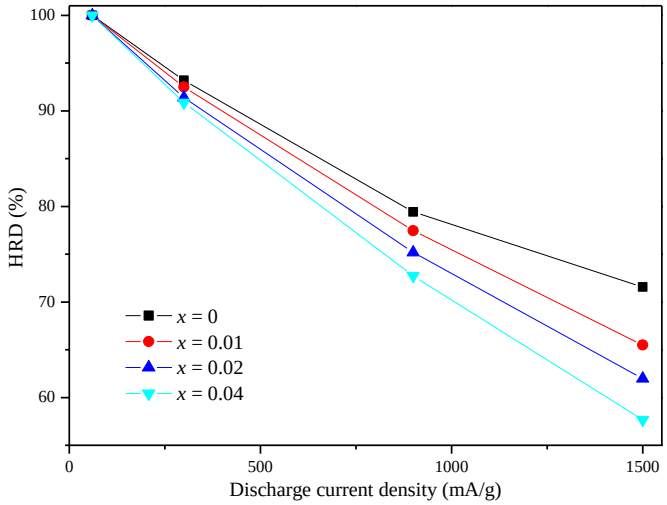

Figure 3. HRD of $La_{0.65-x}Ce_{0.25-x}Pr_{0.03}Nd_{0.07}Y_{2x}Ni_{3.65}Co_{0.75}Mn_{0.3}Al_{0.3}$ alloy electrodes

It is well known that the HRD of the metal-hydride electrodes is dominated by the charge-transfer reaction at the electrode/electrolyte interface and the hydrogen diffusion rate within the bulky alloy electrode, which are reflected in the value of surface exchange current density (I_0), being a

measure of the catalytic activity of an alloy, as well as in the hydrogen diffusion coefficient (D), which characterizes the mass transport properties of an alloy electrode [16].

EIS of $La_{0.65-x}Ce_{0.25-x}Pr_{0.03}Nd_{0.07}Y_{2x}Ni_{3.65}Co_{0.75}Mn_{0.3}Al_{0.3}$ alloy electrodes at 50% DOD are shown in Fig. 4. On the basis of the equivalent circuit[17] and by means of the fitting program Z-View, the R_{ct} values are obtained. The R_{ct} values of the alloy electrodes change little with increasing x value. Furthermore, the exchange current density I_0 can also describe the charge-transfer process. The I_0 value can be calculated according to the following formula [17]:

$$I_0 = \frac{RT}{FR_{ct}} \qquad (1)$$

Where R is the gas constant, T is the absolute temperature, F is the Faraday constant and R_{ct} is the charge-transfer resistance. The I_0 values are calculated by Eq. (1) listed in Table 3. It is clear that the I_0 also changes little with increasing x value. The electrochemical activity of alloy electrode is determined by the amount of electrocatalytic metal on the surface. General, Ni and Co are electrocatalytic metal and can act as the activity site of charge-transfer reaction[16]. The content of Ni and Co do not change, and therefore R_{ct} and I_0 also changes little with increasing x value.

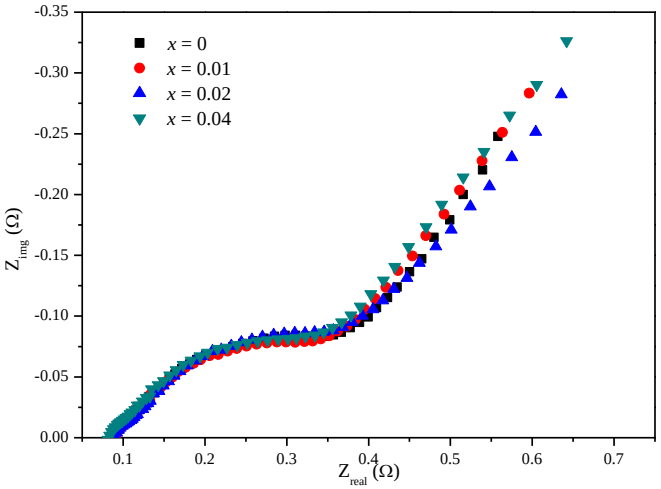

Figure 4. EIS of $La_{0.65-x}Ce_{0.25-x}Pr_{0.03}Nd_{0.07}Y_{2x}Ni_{3.65}Co_{0.75}Mn_{0.3}Al_{0.3}$ alloy electrodes

Table 3. Electrochemical kinetic characteristics of $La_{0.65-x}Ce_{0.25-x}Pr_{0.03}Nd_{0.07}Y_{2x}Ni_{3.65}Co_{0.75}Mn_{0.3}Al_{0.3}$ alloy electrodes

x	R_{ct} (mΩ g)	I_0 (mA/g)	D ($\times 10^{-11}$ cm^2/s)
0	121.2	211.7	12.9
0.01	119.8	214.3	11.8
0.02	120.4	213.3	11.0
0.04	120.5	213.1	10.4

The diffusion coefficient of hydrogen in the alloy electrodes is determined with the potential-step method. Fig. 5 shows the semi-logarithmic plots of the anodic current vs. the time response of $La_{0.65-x}Ce_{0.25-x}Pr_{0.03}Nd_{0.07}Y_{2x}Ni_{3.65}Co_{0.75}Mn_{0.3}Al_{0.3}$ alloy electrodes. Zheng et al. [18] have reported that MH electrode reaction would be controlled by the rate of hydrogen diffusion in the bulk of alloys, when the rate of charge-transfer on the surface of alloy electrodes was so fast that the hydrogen concentration nearly equal to zero under a large anodic potential-step. Assuming that the grains of alloys are all spherical, and the initial hydrogen concentration in the bulk of the alloy is uniform and the hydrogen surface concentration is constant, the hydrogen diffusion coefficient D can be calculated by the slope from the linear plot of lg (i) versus t using the following formula if the discharge time is long enough.

$$\lg i = \lg\left(\frac{6FD}{da^2}(C_0 - C_s)\right) - \frac{\pi^2}{2.303}\frac{D}{a^2}t \qquad (2)$$

where i is anodic current density (A/g), D the hydrogen diffusion coefficient (cm^2/s), d the density of the alloy (g/cm^3), a the radius of the alloy particle, C_0 the initial hydrogen concentration in the bulk of the alloy (mol/cm^3), C_s the surface hydrogen concentration of the alloy (mol/cm^3) and t is the discharge time (s). Assuming that the alloy has a similar particle distribution with an average particle radius of 13 μm according to the previous study [19], D calculated according to the formula above is summarized in Table 3. The D of $La_{0.65-x}Ce_{0.25-x}Pr_{0.03}Nd_{0.07}Y_{2x}Ni_{3.65}Co_{0.75}Mn_{0.3}Al_{0.3}$ alloy electrodes decreases from 12.9×10^{-11} (x = 0) to 10.4×10^{-11} cm^2/s (x = 0.04), which may be ascribed to the following factor. Firstly, as mentioned above, the stability of alloy hydride increases with increasing x value, which is unfavorable to the hydrogen diffusion in the bulky alloy. Secondly, the substation of La and Ce by Y makes the surface oxidation become dense [10], which is detrimental to hydrogen diffusion from inner of the bulk to the surface and then degrades the hydrogen diffusion.

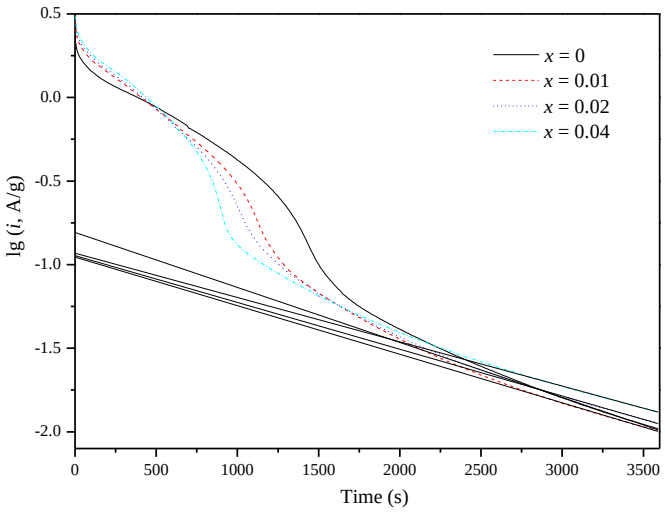

Figure 5. Semilogarithmic curves of anodic current vs. time of response of $La_{0.65-x}Ce_{0.25-x}Pr_{0.03}Nd_{0.07}Y_{2x}Ni_{3.65}Co_{0.75}Mn_{0.3}Al_{0.3}$ alloy electrodes

Iwakura et al. [20, 21] have reported that if the electrochemical kinetics at the electrode/electrolyte interface was rate-determining, a linear dependence of the high-rate dischargeability on the exchange current density should be observed. In contrast, if the diffusion of hydrogen in the alloy was rate-determining, a linear dependence of the high-rate dischargeability on the hydrogen diffusion coefficient should be found. Fig. 6 shows the HRD_{1200} as a function of hydrogen diffusion coefficient for $La_{0.65-x}Ce_{0.25-x}Pr_{0.03}Nd_{0.07}Y_{2x}Ni_{3.65}Co_{0.75}Mn_{0.3}Al_{0.3}$ alloy electrodes. It is evident that the HRD_{1200} increases with the increase in the *D*, and shows a linear relationship with *D*. This implies that the hydrogen diffusion of alloy electrodes should be responsible for the HRD at a discharge current density of 1200 mA/g.

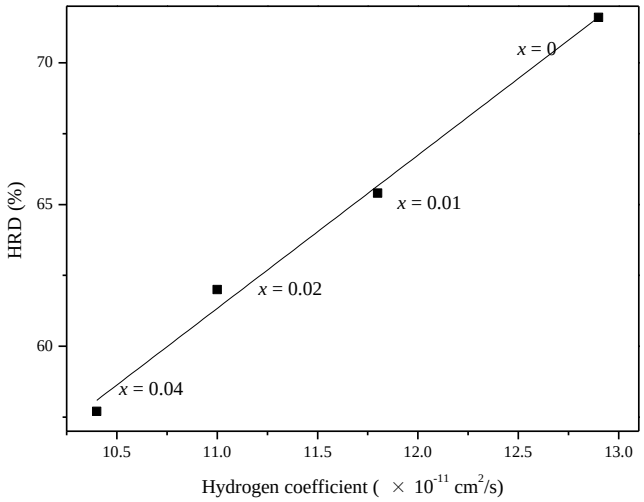

Figure 6. HRD at 1200 mA/g as a function of hydrogen diffusion coefficient for $La_{0.65-x}Ce_{0.25-x}Pr_{0.03}Nd_{0.07}Y_{2x}Ni_{3.65}Co_{0.75}Mn_{0.3}Al_{0.3}$ alloy electrodes

3.4 Cycling stability

The cycle stability is an extremely important factor for the service life of hydrogen storage alloys. The cycling capacity retention rate is expressed as $S_n(\%) = C_n/C_{max} \times 100$ (where C_n is the discharge capacity at the nth cycle). The cycling capacity retention of $La_{0.65-x}Ce_{0.25-x}Pr_{0.03}Nd_{0.07}Y_{2x}Ni_{3.65}Co_{0.75}Mn_{0.3}Al_{0.3}$ alloy electrode as a function of cycle number is shown in Fig. 7. Cycling stability gradually increases with increasing *x* from 0 to 0.0.4. The cycling capacity retention rate after 500 charge/discharge cycles (S_{500}) is listed in Table 2. It can be seen that S_{500} increases from 67.9% (*x* = 0.00) to 80.1% (*x* = 0.04). Generally, the capacity decay of the alloy electrode was ascribed to the pulverization and corrosion [22]. Ticianelli et al. [10] have investigated the degree of corrosion of the $La_{1-x}Y_xNi_{4.7}Sn_{0.3}$ alloys by X-ray absorption spectroscopy, and found that the corrosion resistance increased with increasing *x* value due to the passive film of Y-containing alloys. The corrosion resistance of alloy electrode increases with increasing Y content, which is beneficial to the improvement of cycling stability of alloy electrodes. Unfortunately, Liu et al.[23] pointed out that the larger the unit cell volume resulted in the larger interstitial hole size for hydrogen atoms to occupy.

The larger interstitial hole size, the smaller strain energy that hydrogen atoms to go in and out the crystal. Zhao et al. [24] pointed out that the decrease of the cell volume was unbeneficial to the cycling stability. The *V* of the alloy electrodes decreases with increasing *x* value, which increases the strain energy and degrades anti-pulverization property of the alloy electrodes. This is detrimental to the cycling stability of alloy electrodes. Thus, it is believed that the corrosion resistance is prominent for the improvement of cycling stability of $La_{0.65-x}Ce_{0.25-x}Pr_{0.03}Nd_{0.07}Y_{2x}Ni_{3.65}Co_{0.75}Mn_{0.3}Al_{0.3}$ alloy electrodes in present work.

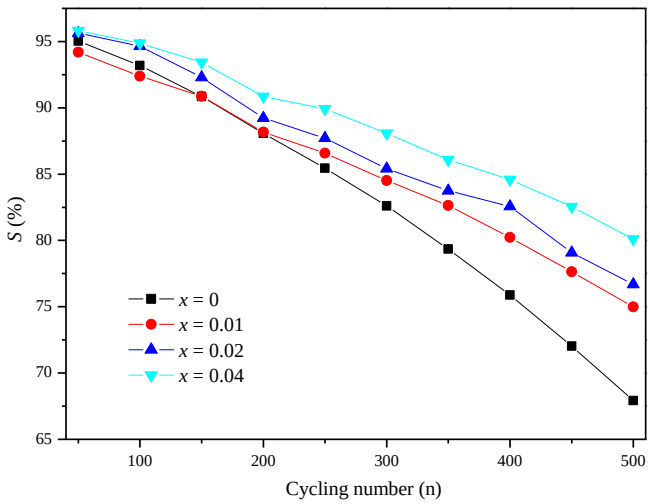

Figure 7. Cycling stability of $La_{0.65-x}Ce_{0.25-x}Pr_{0.03}Nd_{0.07}Y_{2x}Ni_{3.65}Co_{0.75}Mn_{0.3}Al_{0.3}$ alloy electrodes

4 CONCLUSIONS

$La_{0.65-x}Ce_{0.25-x}Pr_{0.03}Nd_{0.07}Y_{2x}Ni_{3.65}Co_{0.75}Mn_{0.3}Al_{0.3}$ alloys are prepared. XRD results indicate that all of the alloys are a single $LaNi_5$ phase. As the *x* value increase in the alloys, the lattice parameter *a*, *c* and cell volume *V* decrease. The activation properties decreases with increasing *x* value. Maximum discharge capacity decreases from 322.95 mAh/g (*x* = 0) to 304.70 mAh/g (*x* = 0.04) with increasing *x* value. HRD_{1200} shows a linear relationship with *D*, implying that the hydrogen diffusion of alloy electrodes should be responsible for the HRD at a discharge current density of 1200 mA/g. Cycling stability gradually increases with increasing *x* from 0 to 0.0.4, which is related with the improvement of corrosion resistance. It is worthy of recognition that the addition of Y is an effective way to improve the cycling stability of AB_5-type alloy as negative electrode in Ni/MH battery.

ACKNOWLEDGMENTS
This research is financially supported by the National Natural Science Foundation of China (51001043), Program for New Century Excellent Talents in University (NCET2011), China Postdoctoral Science Special Foundation (201104390), China Postdoctoral Science Foundation (20100470990), Program for Innovative Research Team (in Science and Technology) in the University

of Henan Province (No. 2012IRTSTHN007), Baotou Science and Technology Project (2011J1003) and the Doctoral Foundation of Henan Polytechnic University (B2010-13).

References

1. T. Sakai, H. Yoshinaga, H. Migamura, N. Kurigama, H. Ishikawa, *J. Alloys Comp.*, 180 (1992) 37
2. F. Feng, M. Geng, D.O. Northwood, *Int. J. Hydrogen Energy*, 26 (2001) 725
3. S. Yang, S. Han, J Song, Y. LI, *J. Rare Earth*, 29 (2011) 692
4. S. Bliznakov, E. Lefterova, N. Dimitrov, K. Petrov, A. Popov, *J. Power Sources*, 176 (2008) 381
5. S.R. Ovshinsky, M.A. Fetcenko, J. Ross, *Science*, 260 (1993) 176
6. B. V. Ratnakumar, C. Witham, R. C. Bowman, Jr., A. Hightower, and B. Fultz, *J. Electrochem. Soc.*, 143 (1996) 2578
7. Y. He, H. Zhang, W.Q. Wu, T.S. Huang, *J. Alloys Compd.*, 312 (2000) 68
8. S. Mukerjee, J. McBreen, J.J. Reilly, J.R. Johnson, G. Adzic, K. Petrov, M.P.S. Kumar, W. Zang, S. Srinivasan, *J. Electrochem. Soc.*, 142 (1995) 2278
9. F. Maurel, P. Leblanc, B. Knosp, M. Backhaus-Ricoult, *J. Alloys Compd.*, 309 (2000) 88
10. E. A. Ticianelli, S. Mukerjee, J. McBreen, G.D. Adzic, J.R. Johnson, J.J. Reilly, *J. Electrochem. Soc.*, 146 (1999) 3582
11. W. Li, Y. L. Du. *Mater. Trans.*, 49 (2008) 2229
12. B. Liu, H. Meng, Y. Fan, L. Li, X. Zhu, A. Li, *Electrochim. Acta*, 69 (2012) 384
13. M. S. Wu, H.R. Wu, Y.Y. Wang, C.C. Wan, *J Alloys Compd.*, 302 (2000) 248
14. R. Brateng, S. Gulbrandsen-Dahl, L.O. VaØen, J.K. Solberg, R. Tunold, *J. Alloys Compd.*, 396 (2005) 100
15. H. Ye, Y.X. Huang, J.X. Chen, H. Zhang, *J. Power Sources*, 103 (2002) 209
16. X.B. Zhang, D.Z. Sun, W.Y. Yin, Y.J. Chai, M.S. Zhao, *ChemPhysChem*, 6 (2005) 520.
17. N. Kuriyama, T. Sakai, H. Miyamura, I. Uehara, H. Ishikawa, *J. Alloys Compd.*, 202 (1993) 183
18. G. Zheng, B.N. Popov, R.E. White, *J. Electrochem. Soc.*, 142 (1995) 2695
19. B.Z. Liu, M.J. Hu, L.Q. Ji, Y.P. Fan, Z. Zhang, A.M. Li, *J. Alloys Compd.*, 516 (2012) 53
20. C. Iwakura, K. Ohkawa, H. Senoh, H. Inoue, *Electrochim. Acta*, 46 (2001) 4383
21. C. Iwakura, M. Miyamoto, H. Inoue, M. Matsuoka, Y. Fukumoto, *J. Alloys Compd.*, 259 (1997) 132
22. D. Chartouni, F. Meli, A. Zuttel, K. Gross, L. Schlapbach, *J. Alloys Compd.*, 241 (1996) 160
23. F.J. Liu, S. Suda, *J. Alloys Compd.*, 232 (1996) 204
24. Y.P. Zhao, Y.H. Zhang, G.Q. Wang, X.P Dong, S.H. Guo, X.L. Wang, *J. Alloys Compd.*, 388 (2005) 284